





# THE NUCLEAR MICROPROBE

## —Investigating Surfaces with Ions

by Carl J. Maggiore

*Focused beams of light ions from a Van de Graaff accelerator nondestructively reveal the three-dimensional distribution of elements in the near surfaces of materials. One hundred times more sensitive than an electron microprobe, the nuclear microprobe has opened up new areas in geologic, biological, metallurgical, and synthetic materials research.*

*Trace-element concentrations in this thin section of rock (200 by 500 micrometers in area) can be determined by the nuclear microprobe with a spatial resolution of 1 micrometer and a sensitivity of 1 to 10 parts per million. Such spatially resolved data for the two dark sphene crystals at the center of the micrograph provide information about the cooling rates during their formation. The perfect crystal shape indicates that the sphene was the first mineral to crystallize from a magma, incorporating into its structure many trace elements, such as thorium, uranium, and the rare earths. Knowledge of trace-element concentrations in the surrounding granitic rock (feldspars, quartz, and biotite) are useful for many applications, including geothermal energy, solution mining, waste isolation, and modeling ore-body formation. The optical micrograph was taken (with crossed polarizers and a color-enhancing quarter-wave plate) by Rosemary Vidale of the Laboratory's Isotope Geochemistry Group.*

**B**asic to any study of a material is knowledge of what elements it contains and how they are distributed. This knowledge is particularly important for the thin layer near the surface of a solid, where trace-element distributions determine such macroscopic properties as electrical conductivity, chemical reactivity, hardness, and wear resistance. Trace-element distributions are also the key to dating mineral specimens from the earth and from space and to understanding the processes of their formation.

Over the past twenty years a number of new techniques and instruments have been developed to analyze the near-surface region. These include Auger analysis, the electron microprobe, photoelectron spectroscopy, the laser microprobe, secondary-ion mass spectrometry, and scattered-ion spectrometry. Each in its own manner, be it destructive or nondestructive, provides either qualitative or quantitative information about the elemental or chemical nature of the near surface.

Among these the nuclear microprobe has several features that make it a unique instrument for analyzing the near-surface region. It is nondestructive; it is sensitive to trace elements and to monolayer of heavy elements; it has a spatial resolution of a few micrometers; it

yields quantitative information about the elements present as well as their depth profiles; and, finally, interpretation of the data is relatively easy and unambiguous. The nuclear microprobe is designed to irradiate the near surface of a specimen with a focused beam of light ions and detect at each point the backscattered ions, nuclear reaction products, and x rays that result from interaction of the incident beam with the specimen. Analysis of these signals yields three-dimensional distributions of elements in a region less than 10 micrometers ( $\mu\text{m}$ ) deep.

At present there are about ten nuclear microprobe in the world, of which the Los Alamos microprobe has the most intense beam and the potential for the highest spatial resolution. As the beam from the Laboratory's vertical Van de Graaff accelerator passes through an elaborate focusing system, it is fashioned into a very fine stream of nearly monoenergetic ions. The unique feature of this system is the final focusing device, a superconducting solenoid lens specially designed to focus the maximum current into the smallest spot.

The initial motivation for developing this sophisticated microprobe was the examination of new types of compound semiconductor devices. The localized distribution of impurities in these small objects is the key to their electrical properties. This application has been only a starting point. We are currently exploiting the sensitivity and spatial resolution of the microprobe to measure the density of thin-film targets for equation-of-state studies, catalyst migration in fuel cells, and trace-element concentrations in geologic materials. This instrument is opening up to detailed materials analysis the world with dimensions below  $5 \mu\text{m}$ .

### Nuclear Microprobe Signals

By the usual standards of surface physics, an incident ion with an energy of a few million electron volts (MeV) presents an

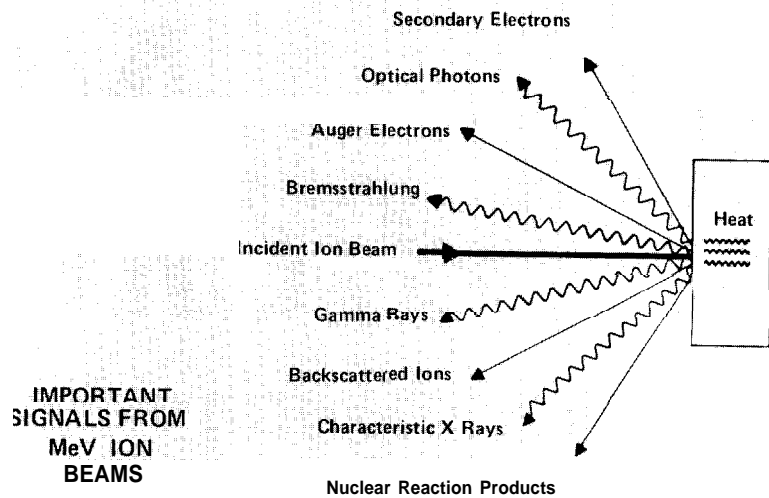


Fig. 1. Possible results of the interaction of few-MeV light ions with a specimen.

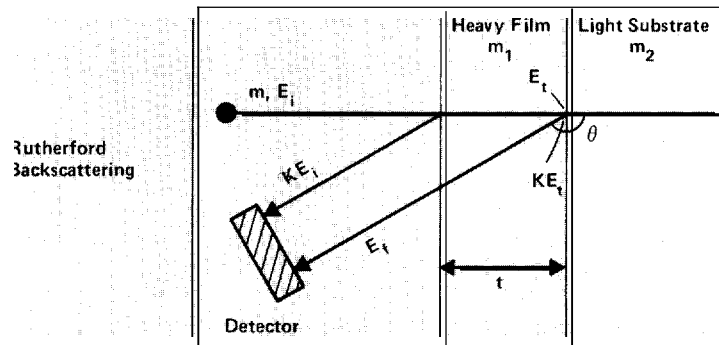
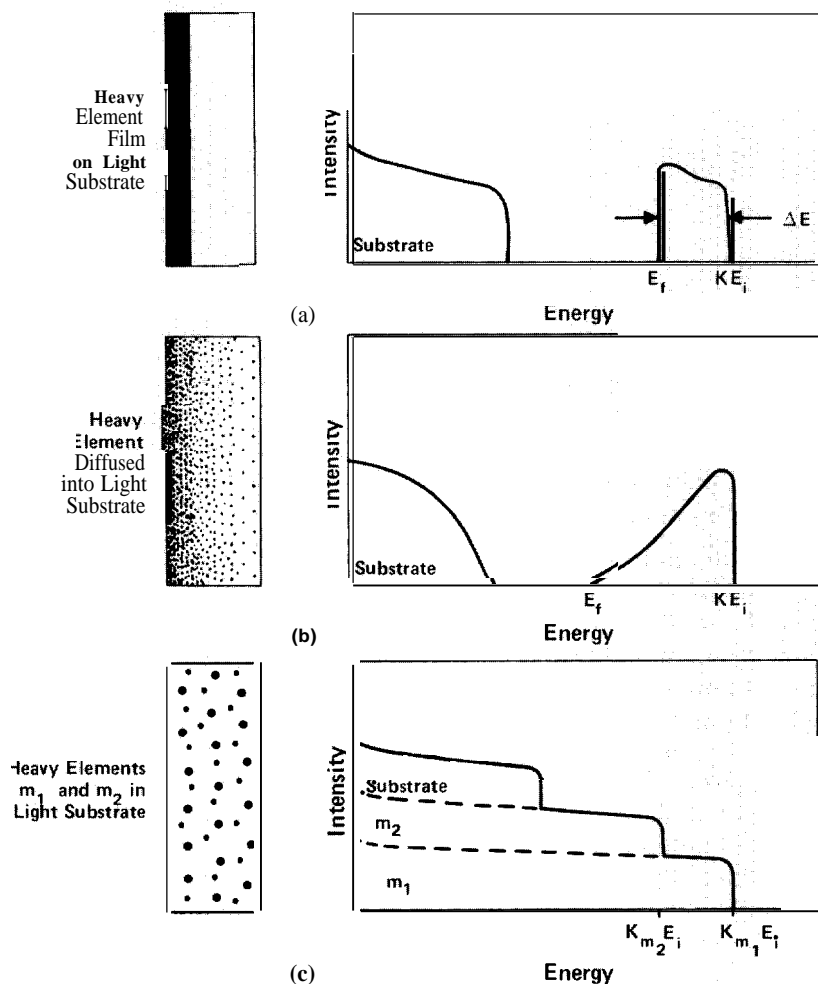


Fig. 2. Setup for a Rutherford backscattering experiment. Incident ions of mass  $m$  and energy  $E_i$  are scattered by nuclei of mass  $m_1$  in a heavy-element film on a light-element substrate. A detector at an angle  $\theta$  relative to the direction of the incident ions records the number and final energies of ions backscattered through  $\theta$ . The final energy of ions backscattered from the surface of the film is  $KE_f$ , where  $K$  is the kinematic factor defined in the text. Also shown are ions backscattered through  $\theta$  from the deepest part of the film. These ions lose energy by traveling into the film, by scattering, and by traveling out of the film. Therefore, their energy at the time of scattering,  $E_s$ , is less than  $E_i$ , and their final energy  $E_f$  recorded by the detector is related not only to the mass of the scattering nucleus but also to the depth at which scattering occurred. Ions scattered by the light elements of mass  $m_2$  in the substrate have distinctly lower energies than ions scattered from the heavy-element film.



**Fig. 3.** (a) Rutherford backscattering spectrum of the specimen depicted in Fig. 2, a heavy-element film on a light-element substrate. The mass  $m_1$  of the heavy element can be deduced from  $KE_i$ . The thickness of the film can be deduced from  $\Delta E = KE_i - E_f$  if the energy losses of the ion per unit path length in the heavy element film are known. (b) Backscattering spectrum of a heavy element diffused into a light-element substrate. The height of the heavy element's backscattering peak declines rapidly with decreasing energy. This decline indicates that the concentration of the heavy element decreases rapidly with depth. (c) Backscattering spectrum from a light-element substrate in which two heavy elements are uniformly distributed. The mass of each heavy element can be determined from the high-energy edges of the steps and the concentration is found from the step heights.

enormous perturbation to the specimen being examined. Figure 1 shows some results of the interaction between a beam of light ions (protons, deuterons, tritons, helium-3 ions, or alpha particles) and the specimen's near surface. The multiplicity of results is due to the relatively high energy of the incident ions. The three signals of primary interest for a nuclear microprobe are backscattered ions, nuclear reaction products, including gamma rays, and characteristic x rays. In combination these signals permit quantitative measurement of the near-surface distribution of

almost all elements. The perturbations of the system, particularly radiation damage, constitute a major limitation on the use of the nuclear microprobe, but for many applications the information sought can be obtained without destroying it by the act of measurement.

**BACK SCATTERED IONS.** An ion passing through a specimen undergoes elastic scattering as its Coulomb (electrical) field interacts with that of an atomic nucleus in the specimen. (The scattering is elastic in the

sense that the total kinetic energy of the scattering ion and the scattering nucleus remains constant during the interaction.) The process is often called Rutherford scattering in honor of Ernest Rutherford, who was led to his nuclear model of the atom by the fact that some small fraction of the incident ions are backscattered, that is, scattered through angles greater than  $90^\circ$  relative to the initial direction of the ions. Since the cross section, or probability, for Rutherford scattering increases with the square of the charge of the scattering nucleus, ions are more likely to be scattered by the heavier element(s) in a specimen. Therefore, as an analysis technique Rutherford scattering is particularly applicable to specimens consisting of heavy elements distributed within a light-element medium.

The specimens investigated with the nuclear microprobe are usually so thick that the ions scattered in the forward direction come to rest within the specimen. It is only the backscattered ions that escape to tell the tale about the masses, numbers, and locations of the heavy nuclei distributed within the near surface of a light-element medium. A simple experimental setup to determine these quantities is shown in Fig. 2. Ions of known mass  $m$  and initial energy  $E_i$  are directed at a specimen consisting of a heavy-element film on a light-element substrate, and a suitable detector, such as a silicon surface-barrier detector, measures the number and final energies of ions scattered through an angle  $\theta$  close to  $180^\circ$ . Because the ions lose energy not only by backscattering but also by other interactions as they enter and leave the specimen, all the ions backscattered through  $\theta$  do not have the same final energy. Rather the detector records a spectrum of energies whose values depend on the mass of the scattering nucleus and on the depths at which the backscattering occurred.

The maximum energy in the spectrum is the energy  $E'$  of those ions backscattered at the surface of the specimen. Energy and

momentum conservation in the scattering process determine that  $E' = KE_i$ , where  $K$ , the so-called kinematic factor, is given by

$$K = \frac{m \cos \theta + (m_1^2 - m^2 \sin^2 \theta)^{1/2}}{m + m_1}$$

and  $m_1$  is the mass of the heavy element. We can thus determine  $m_1$  by using this kinematic relation and the known values of  $E_i$ ,  $m$ ,  $\theta$ , and  $E'$ .

Ions **backscattered** at some depth within the heavy-element film suffer additional energy losses in traveling into and out of the specimen. Since these losses are known as a function of path length and compiled in the literature, we can infer information about the depth distribution of the scattering nuclei from the energy spectrum. The energy losses per unit path length are primarily due to interactions with the electrons in the specimen and vary with the energy of the incident ions. For maximum depth sensitivity the energy of the incident ions should be near the energy at which the energy loss per unit path length is a maximum. This energy is, for example, about **1 MeV** for alpha particles in a specimen of medium atomic weight.

The incident ions also **backscatter** from the light-element substrate. These **backscattered** ions have transferred more energy and momentum to the lighter scattering nuclei and therefore have lower energies.

Figure 3 shows some typical energy spectra of **backscattered** ions. Different spectral shapes are characteristic of different depth profiles, such as a heavy-element film on a light-element substrate, two heavy elements uniformly distributed in a light-element matrix, or one heavy element unevenly distributed in a light-element matrix. The shapes of the peaks may horrify a nuclear spectroscopist, but, together with the intensities, they contain enough information to yield elemental concentration versus depth with a depth resolution less than  $0.02 \mu\text{m}$  at normal incidence.

These **backscattering** measurements are particularly suited to studies of thin films and surface contamination. They are also useful for determining elemental depth profiles of doped materials and of compound materials whose composition changes with depth.

**NUCLEAR REACTION PRODUCTS.** Because the cross section for Rutherford scattering is much larger for heavy elements than for light elements, **backscattering** measurements are not sensitive to light elements in a heavy-element matrix. However, nature has obligingly provided a complementary interaction for specimens of this type, namely nuclear reactions. Incident ions with energies of a few **MeV** can penetrate the lower Coulomb barrier of the light nuclei and react through nuclear forces to create different light ions.

For materials analysis with ion beams, the nuclear reaction must have a high cross section and be free of interferences. Moreover, the reaction must liberate enough kinetic energy that the light-ion products can reach the detector. Fortunately, numerous reactions are suitable. Some common ones involve the reaction of incident **deuterons** to produce protons or alpha particles or of incident protons to produce alpha particles or gamma rays. These and other reactions of light elements have been well studied by nuclear spectroscopists over the past thirty years; therefore, an adequate data base exists for determining elemental composition from the microprobe data. Depth information is also contained in the data, for the incident ions and reaction products undergo the same type of energy loss in traveling through the sample as was described above for Rutherford scattering. Since nuclear reactions are sensitive to isotopic composition, the nuclear microprobe offers many possibilities for tracer studies with stable isotopes. Further, the nuclear microprobe is unique among near-surface analytical methods in being able to determine quantitatively the depth distributions of hydrogen, deuterium, and tritium.

The energies required to induce nuclear reactions are typically less than **3 MeV**, and the reaction products are detected with the same surface-barrier detector used to detect **backscattered** ions.

**CHARACTERISTIC X RAYS.** X rays are the third analytical signal readily available from the nuclear microprobe. These x rays are the result of interactions between the incident ions and atomic electrons in the specimen. The electrons are excited to higher energy levels and eventually return to the ground state, emitting x rays with an energy characteristic of the element involved. A lithium-drifted silicon detector can be used to detect the x rays and measure their energy.

Operated in this manner, the nuclear microprobe functions exactly like an electron microprobe but has an important advantage. Because the mass of even a light ion is much greater (by a factor of 1800 or more) than that of an electron, the background **bremsstrahlung** is reduced considerably. Consequently, the nuclear microprobe can detect elements at concentrations between 1 and 10 parts per million, whereas the electron microprobe is limited to concentrations of about 1000 parts per million. This increase in sensitivity by a factor of 100 or more has opened up important areas of materials research in biology and geochemistry.

Although the x-ray data does not yield any depth information, it does provide a complement to the depth profiles obtained from **backscattering** spectra. For example, **backscattering** data may be ambiguous for heavy elements whose mass differences are small. In such cases data from an x-ray spectrometer, which easily distinguishes adjacent elements in the periodic table, can be used to resolve ambiguities in the **backscattering** spectra.

#### Design Considerations for High Spatial Resolution

All three analysis methods described

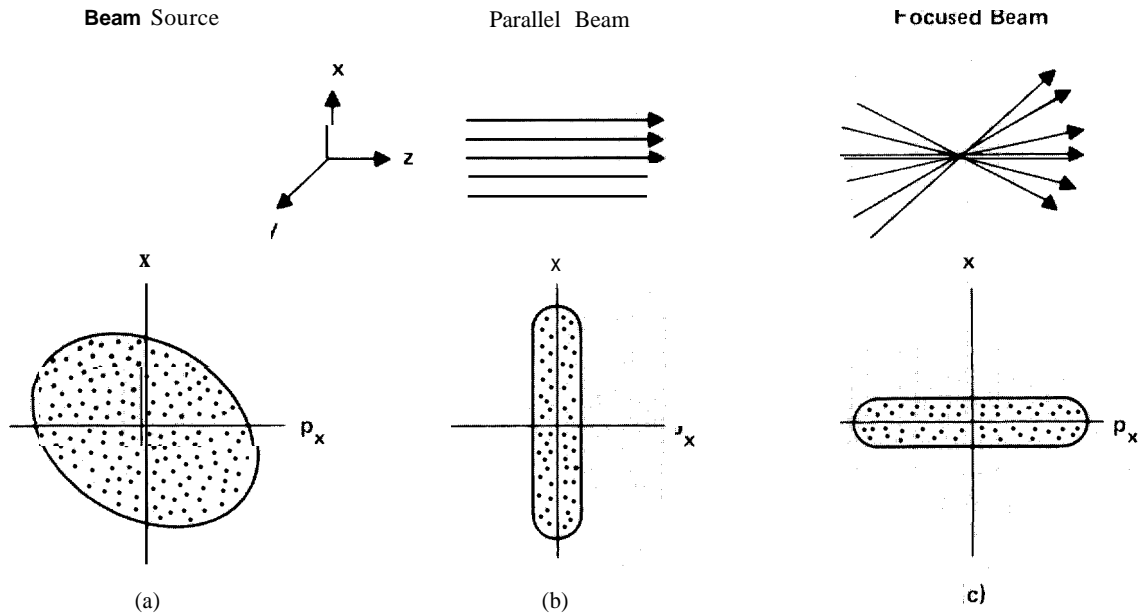


Fig. 4. The phase space occupied by a system of particles is defined by their spatial  $(x,y,z)$  and momentum  $(p_x,p_y,p_z)$  coordinates. The figure shows the  $xp_x$  plane of the phase space occupied by a beam of ions traveling in the  $z$  direction. Three beam configurations are depicted: (a) a typical ion source, such as a Van de Graaff accelerator, in which the ions have a substantial spread in both space and momentum; (b) a parallel

beam in which the ions are spread in the  $x$  direction but have almost no momentum in that direction; and (c) a crossover point where the beam has almost no spatial extent but has a large spread in momentum. Focusing devices can change the shape and area of the phase space occupied by the beam but cannot change the density of points in phase space.

above are well known and well documented in the literature. Moreover, if a sample is uniform over dimensions of a few square millimeters, the methods yield satisfactory results with a direct beam line from any Van de Graaff accelerator. But specimens of technological interest are rarely uniform over these dimensions. Typical structures in semiconductor devices have dimensions of  $5 \mu\text{m}$  or less; separate phases and grains in mineralogical specimens are a few micrometers in diameter; cracks and grain boundaries in solids have dimensions of  $1 \mu\text{m}$  or less; biological structures of interest are often less than a few micrometers in size; and the average "dust" particle has dimensions of a few micrometers. The challenge we faced was to fashion a Van de Graaff ion beam into a tool for nondestructive analysis of this world below  $5 \mu\text{m}$ .

A Van de Graaff accelerator is an appropriate ion source for two reasons: it can accelerate the variety of ions we need for different applications, and it produces a high-current beam with good energy regulation. However, to use a Van de Graaff beam in much the same way that scientists use an electron microscope, we must consider ques-

tions of spatial resolution, sensitivity, and radiation damage.

**SPATIAL RESOLUTION AND SENSITIVITY.** To achieve spatial resolution of a micrometer or two, the beam must be focused to a spot of this dimension. At the same time the current in the spot must be sufficient to generate a measurable signal in a reasonably short time.

The final spot size and current are not independent quantities but instead are related to the characteristics of the ion source through Liouville's theorem about transformations of the phase space occupied by a system of particles. [The phase space occupied by a system of particles consists of the spatial  $(x,y,z)$  and momentum  $(p_x,p_y,p_z)$  coordinates of the particles.] The area of phase space occupied in the  $xp_x$  plane by a beam of ions traveling in the  $z$  direction is a bounded region with a certain density of points (Fig. 4). Liouville's theorem states that any transformation of a bounded region of phase space does not change the density of points in that phase space. In other words, focusing elements and emittance-limiting elements may be placed in the beam line to

produce a small spot, but the phase-space density of the particles in that spot cannot be increased beyond that of the source. This theorem places an upper limit on the current in the final spot ( $i_{\text{spot}}$ ) in terms of the current of the accelerator beam ( $i_{\text{source}}$ ):

$$i_{\text{spot}} \leq \frac{(\epsilon_x \epsilon_y)_{\text{spot}}}{(\epsilon_x \epsilon_y)_{\text{source}}} i_{\text{source}}$$

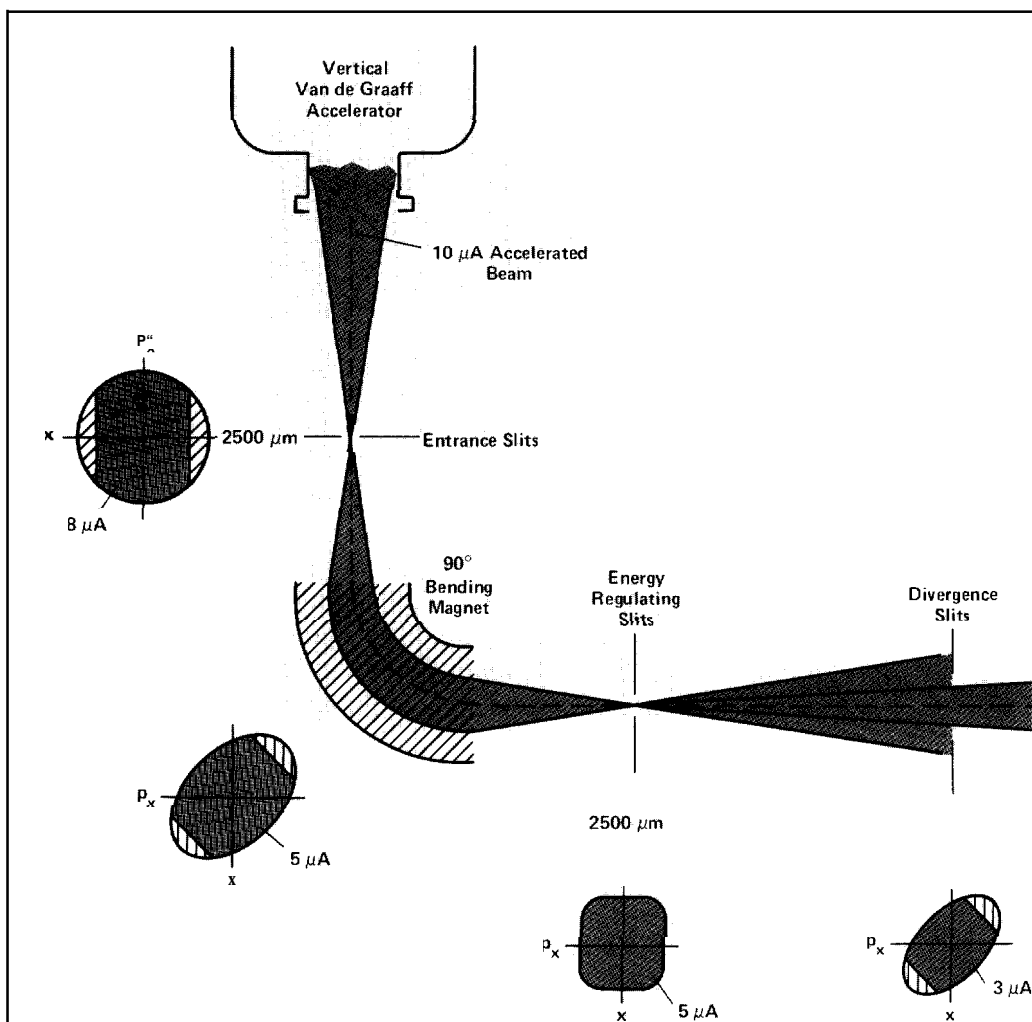
where the normalized emittance  $\epsilon$  is a measure of the phase space occupied by the beam in units of length times angle times  $(\text{energy})^{1/2}$ . To estimate  $\epsilon_{\text{source}}$ , we assume a spot size approximately  $1 \mu\text{m}$  in diameter and a semidivergence (angular spread) for the beam of 20 milliradians. With a semidivergence of this magnitude, we can still maintain a spatial resolution of  $1 \mu\text{m}$  in the near-surface region of the sample. The theoretical limit on the current in the spot also depends on the normalized emittance and current of the ion source. For a Van de Graaff accelerator with a duoplasmatron ion source, the typical normalized emittance is 1 to 10 millimeters milliradians  $(\text{MeV})^{1/2}$  and the maximum beam current is 10 micro-

amperes. With these numbers we obtain 4 nanoamperes as the maximum current in a 1- $\mu\text{m}$ -diameter spot.

Although optical aberrations in the focusing and emittance-limiting devices may reduce this theoretical limit by a factor of 100, the final current is nevertheless more than sufficient to produce adequate signals in the detector. In fact, some experiments are possible with currents in the picoampere range, and 4-nanoampere currents produce count rates that approach and can exceed the limitations of backscatter and x-ray detectors. Of course, a lower-current beam spot must probe a specimen for a longer time to measure its elemental composition. Typically, an incident charge of 1 microcoulomb is needed to detect either a monolayer of a heavy element or an elemental concentration of 1 to 10 parts per million.

**RADIATION DAMAGE.** Radiation damage is, of course, a broad term referring to everything from the Generation of color centers in alkali halides to the formation of blisters in metals. In microprobe experiments radiation damage refers to a change in a specimen's elemental distribution caused by the ion beam being used to measure that distribution. There are two effects that can move atoms over distances comparable to the microprobe's spatial resolution, thermal diffusion and nuclear recoil.

**Thermal Diffusion.** Localized heating of the sample during irradiation can lead to diffusion of ions out of the sampling area. The local temperature will depend on the thermal conductivity of the specimen. Since most metals and semiconductors have thermal conductivities greater than 0.1 calorie per centimeter second degree, the temperature increase in the irradiated region will be 10 kelvins or less and will not be a problem for specimens of this type. Glasses and biological specimens, however, have much smaller thermal conductivities, 0.01 calorie per centimeter second degree or less. Consequently, irradiation of these materials may



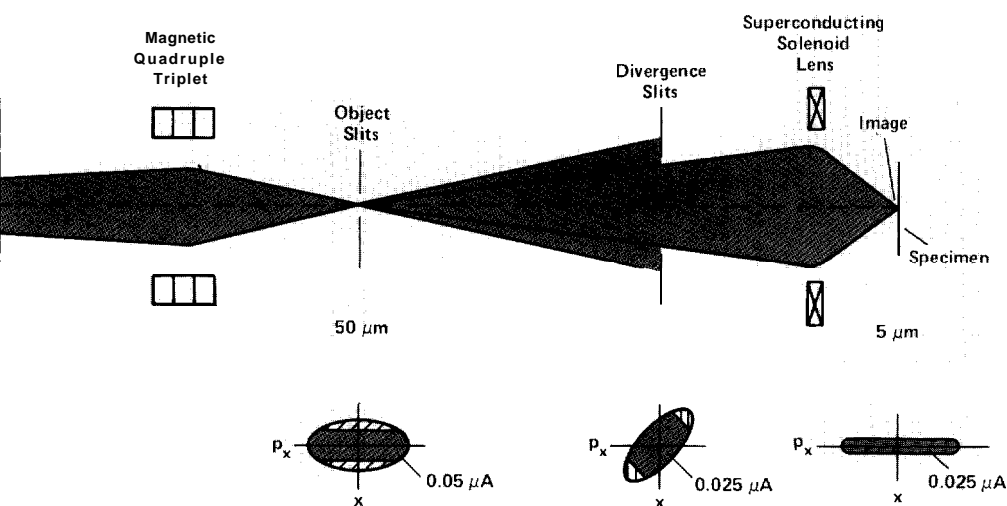
*The beam line of the Los Alamos nuclear microprobe is designed to focus the maximum current into a small-diameter spot. The phase-space plots show how each of the various focusing and emittance-limiting elements reshapes the beam. The cross-hatched areas of the phase-space plots represent those parts of the beam discarded by the element. Each phase-space plot is labeled with the current and diameter of the beam at that point. The finite bore of the 90° bending magnet limits the high-divergence ions in the beam. The energy-regulating slits (the exit slits of the 90° magnet) do not limit the beam's phase space if the energy of the ions is constant;*

lead to a local temperature increase of several hundred kelvins, diffusion, and a change in the elemental distribution.

**Nuclear Recoils.** Rutherford scattering can impart a significant amount of kinetic energy to the scattering nuclei. For example, if an incident alpha particle with an energy of a

few MeV scatters directly backward, the scattering nucleus recoils in the forward direction with an energy greater than 0.1 MeV. The range of the recoiling nucleus depends on its energy, mass, charge, and the matrix, but typically it will move from 0.1 to 1.0  $\mu\text{m}$  farther into the sample. This displacement is much greater than the depth

## Los Alamos Microprobe Beam Line



however, if the energy changes, the beam shifts relative to the slits and the amount of current through the rest of the beam line decreases. The first set of divergence slits limits the beam entering the quadrupole triplet. This lens brings the beam to a crossover at the object slits, which define the size of the beam to be demagnified by the final lens. Approximately 95 per cent of the beam is thrown away at this point. The final set of divergence slits limits the high-divergence ions entering the final superconducting solenoid lens. This lens brings the beam to a focus at the specimen. In general, a small spot size is obtained by increasing the divergence of the beam.

resolution (0.02  $\mu\text{m}$ ) of backscattering experiments. Thus, the measurement process can significantly perturb the depth distribution of some fraction of the nuclei in the sample.

We can estimate this fraction for an experiment involving, say, irradiation of a 1- $\mu\text{m}^2$  area of a gold monolayer with a beam of

$6.25 \times 10^{12}$  singly charged, 1-MeV helium-4 ions, that is, with 1 microcoulomb of incident charge (Fig. 5). We assume that only the ions scattered through a laboratory angle greater than  $90^\circ$  cause significant displacement of the scattering nuclei in the forward direction. (The majority of ions are scattered through the forward hemisphere and do not

impart sufficient tangential momentum to the scattering nuclei to displace them laterally from the sampling area.) We can easily calculate the total number  $A$  of ions that cause significant displacement by integrating the Rutherford cross section over the backward hemisphere. We perform the integration in the center-of-mass frame and assume that the center-of-mass scattering angle is equal to the laboratory scattering angle. (This assumption is valid when the scattering nuclei are much more massive than the scattered nuclei.) Then

$$A = 2\pi QNt \left( \frac{ZZ' e^2}{4E} \right)^2 \int_{\pi/2}^{\pi} \frac{\sin \theta}{\sin^4(\theta/2)} d\theta$$

where  $Q$  is the number of incident ions,  $Nt$  is the areal number density of the monolayer ( $1.8 \times 10^{15}$  nuclei per square centimeter),  $Z$  and  $Z'$  are the atomic numbers of the gold nuclei and the helium-4 ions,  $e$  is the charge of the electron, and  $E$  is the incident energy of the ions. Evaluating this expression we find that  $A$  is  $4.6 \times 10^6$ . Each of these ions scattered through an angle greater than  $90^\circ$  has produced a significant forward displacement of a gold nucleus. The number of gold nuclei irradiated is the product of the monolayer's areal number density and the irradiated area, or  $1.8 \times 10^7$ . Thus 25 per cent of the gold nuclei are significantly displaced.

In a similar fashion we can calculate the number of backscattered ions that are detected in this experiment, assuming that the detector has an angular acceptance of  $10^{-3}$  steradians and is located at an angle of 1750 relative to the incident beam. From this number, 360, we learn that the statistical accuracy of the measurement is about 5 per cent. Thus, 25 per cent of the gold nuclei are significantly displaced by a measurement with a statistical accuracy of 5 per cent. Such a measurement would have altered the specimen by an amount greater than the statistical accuracy of the measurement. To avoid this problem we must increase the beam spot size or be content with lower

accuracy. Nuclear recoils represent an ultimate limitation on microprobe experiments; they can, however, be tolerated in many applications.

### Los Alamos Microprobe Beam Line

Microprobe measurements with spatial resolution of a few square micrometers are worth pursuing provided the data-acquisition times are reasonable. These times depend on how fast the beam can deliver probing ions to the target area. A beam current density of 50 picoamperes per  $\mu\text{m}^2$  requires a rather long data-acquisition time (about 300 minutes) if 1 microcoulomb of charge is needed. At 1 nanoampere per  $\mu\text{m}^2$  the time required reduces to 15 minutes and becomes more manageable. Therefore, our goal in designing the microprobe beam line and final lens was to maximize the current density in the final spot.

The figure on pages 32 and 33 depicts the microprobe beam line at the Laboratory's vertical Van de Graaff accelerator. Most of the beam-line elements are common to all nuclear microprobe. A  $90^\circ$  bending magnet with variable entrance and exit slits regulates the energy of the ions in the beam by transmitting ions of the correct energy. A quadruple triplet changes the divergence of the beam to match the angular acceptance of the final lens, and two pairs of crossed microslits define the object that is to be demagnified by the final lens. The unique element in the Los Alamos microprobe is the superconducting solenoid lens that is designed to focus the maximum current density into the final spot.

To focus a relatively large volume of phase space into a small spot requires a lens with a large angular acceptance and a short focal length. The short focal length can be provided by a multiplet of magnetic or electric quadruples, the standard lenses for focusing light ions with energies of a few MeV. A multiplet is needed because a single quadruple produces a nonaxially symmetric field that is converging in one plane and

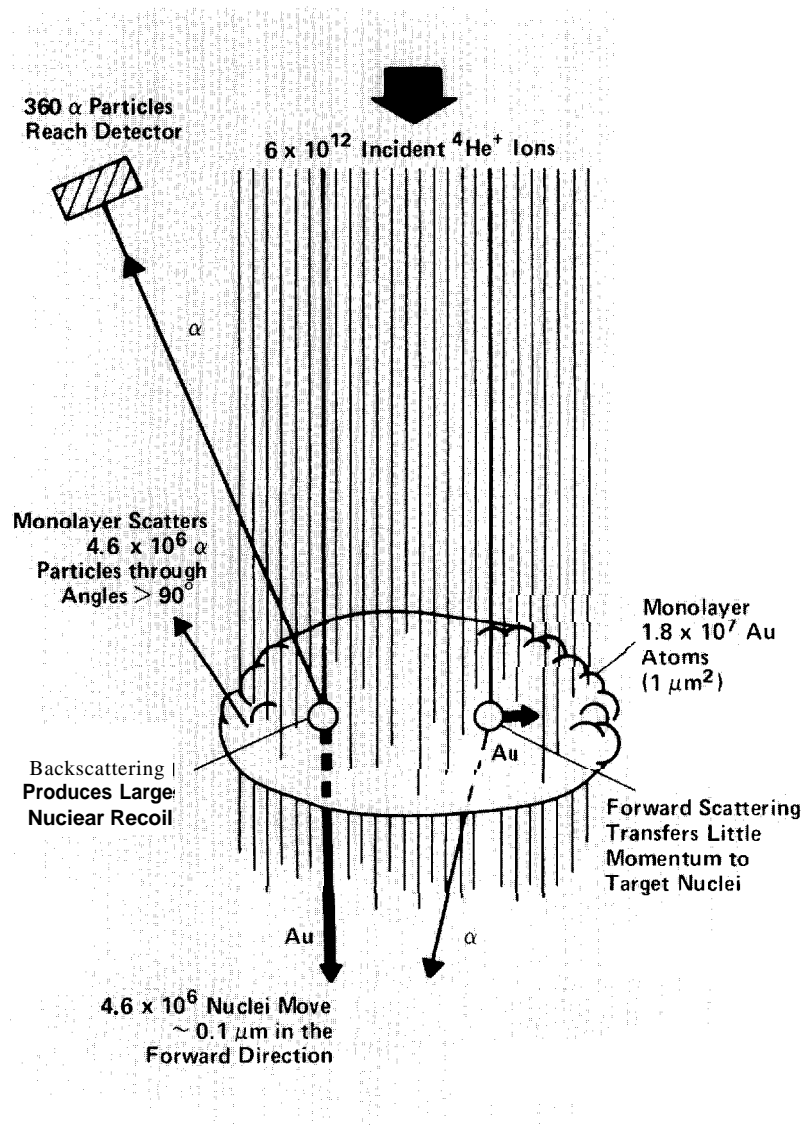


**Fig. 5. Nuclear recoils in backscattering experiments.** When  $6 \times 10^{12}$   ${}^4\text{He}^+$  ions (1 microcoulomb of charge) are incident on a monolayer of gold atoms, about 360 ions will scatter into a  $10^{-3}$ -steradian detector at a  $175^\circ$  angle relative to the incident direction. The target area ( $1 \mu\text{m}^2$ ) contains  $1.8 \times 10^7$  gold atoms. Most of the incident ions pass through the target. Those that scatter in the forward direction transfer only a small amount of momentum to the scattering nuclei. But about  $4.6 \times 10^6$  ions scatter through an angle greater than  $90^\circ$  and transfer enough forward momentum to the scattering nuclei to measurably change their depth. Thus detecting the presence of a monolayer of gold atoms with a statistical accuracy of about 5 per cent will move 25 per cent of the gold atoms a measurable distance (about  $0.1 \mu\text{m}$ ) deeper into the sample.

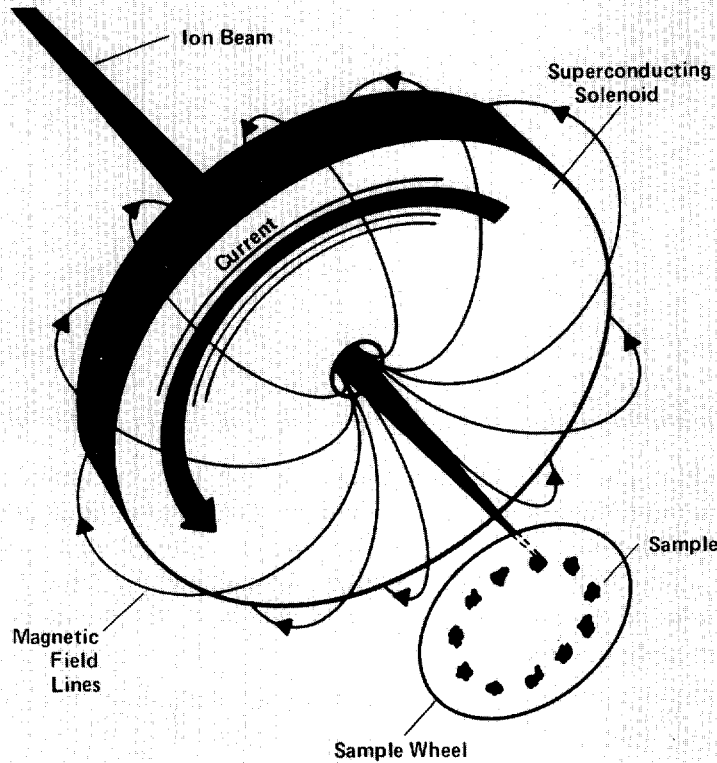


**Fig. 6.** Focusing action of the superconducting solenoid lens. A 70-ampere current flows through the windings of the pancake-shaped solenoid (5 centimeters thick and 30 centimeters in diameter) to produce an 80-kilogauss field in the lens's room-temperature bore. This field is high enough to focus few-Me V light ions onto a sample 10 centimeters from the center of the lens. To maintain the solenoid at superconducting temperatures, it is contained in a Dewar of liquid helium. Specifications of the solenoid lens are listed in Table I.

diverging in the orthogonal plane. A doublet, triplet, or quadruplet of quadrupoles can produce a converging lens, but to obtain a spot size approaching 1  $\mu\text{m}$  in diameter requires very good electrical, magnetic, and mechanical uniformity. Consequently, design and construction of the quadrupoles demands great care.

We chose instead the conceptual simplicity of a solenoid lens. Its concentric circles of electric current produce an axially symmetric magnetic field whose focusing action is everywhere converging. The angular acceptance of a solenoid lens is limited only by the bore of the magnet. However, a solenoid lens is only weakly focusing and therefore requires much higher magnetic fields than do quadrupoles to produce a short focal length. In fact, the 80-kilogauss fields required to focus ions with energies up to 6 MeV cannot be produced with conventional technology. Long before such strong fields are attained, the high currents required would melt the solenoid wires and an iron core inserted to concentrate the field lines would saturate and be useless. Therefore, we combined the conceptual simplicity of the solenoid with the sophisticated technology of superconductivity. Cooled by liquid helium to temperatures at which its resistance drops to zero, the solenoid can sustain a current of 70 amperes through its windings to produce field strengths of 80 kilogauss. Figure 6 shows the focusing action of the superconducting solenoid lens, and Table I lists its specifications.

The magnetic field produced in the room-temperature bore of the lens is a close approximation to the Glaser field given by

$$B(z) = \frac{B_0}{1 + \left(\frac{z}{a}\right)^2},$$

where  $B_0$  is the field strength at the center of the lens,  $z$  is the distance in centimeters along the axis from the center of the lens, and  $a = 6.5$  centimeters.

The solenoid lens is not a perfect focusing

**TABLE I**  
**SUPERCONDUCTING SOLENOID LENS CHARACTERISTICS**

Type	Multifilament NbTi NbTi:Cu = 1:1.3 Epoxy potted
Dimensions	5-cm bore length Three-stage winding $r_1 = 2.50$ cm $r_2 = 5.75$ cm $r_3 = 9.65$ cm $r_4 = 15.80$ cm
Maximum current density	Stage 1: $1.01 \times 10^4$ A/cm <sup>2</sup> Stage 2: $1.43 \times 10^4$ A/cm <sup>2</sup> Stage 3: $2.46 \times 10^4$ A/cm <sup>2</sup>
Maximum current	69.56 A
Maximum field on axis	80 kG
Liquid helium consumption	1.5 l/h at maximum field
Inductance	45.2 H
Manufacturer	Intermagnetics General

device but instead has various aberrations that enlarge the beam spot. The dominant ones are spherical and chromatic aberrations. Spherical aberrations (Fig. 7) arise because the focusing action on ions far from the axis of the lens is stronger than on ions near the axis. Spherical aberrations cause the focused beam to have a diameter  $d_s$  given by

$$d_s = \frac{C_s}{2} \alpha^3,$$

where  $C_s$  is the spherical aberration coefficient and  $\alpha$  is the semidivergence.

Chromatic aberrations result from the inability of the lens to focus ions with different energies to the same spot. As shown in Fig. 8, the less energetic ions are bent more sharply and are therefore focused at a shorter distance from the lens. The spot diameter due to chromatic aberrations is given by

$$d_c = 2C_c \alpha \frac{\Delta E}{E},$$

where  $C_c$  is the chromatic aberration coefficient and  $\Delta E/E$  is the energy variation in the beam. At present the energy variation is about 1 part in  $10^3$ .

The aberration coefficients are related to the properties of the lens and are usually very difficult to compute, but because the field of the solenoid lens approximates the Glaser field, we were able to calculate these coefficients analytically. Then, assuming that the effects of these aberrations add in quadrature, we calculated the beam current versus spot size for the superconducting solenoid lens (Fig. 9). From these calculations we drew the following conclusions.

- Current densities approaching 1 nanoampere per  $\mu\text{m}^2$  in the focused spot are possible.

- Chromatic aberrations cause the greatest increase in the diameter of the focused spot. Therefore, energy regulation of 1 part in  $10^4$  will be necessary to achieve submicrometer spatial resolution.

- The current densities associated with submicrometer spatial resolution will probably be useful only for inducing x-ray emission.

Since chromatic aberrations impose a fundamental limitation on the beam-spot size, we have attempted to improve the energy regulation of the accelerator at low energies. These efforts have not been particularly successful. But the fact that small variations in the energy of the incident beam do not

### Spherical Aberration

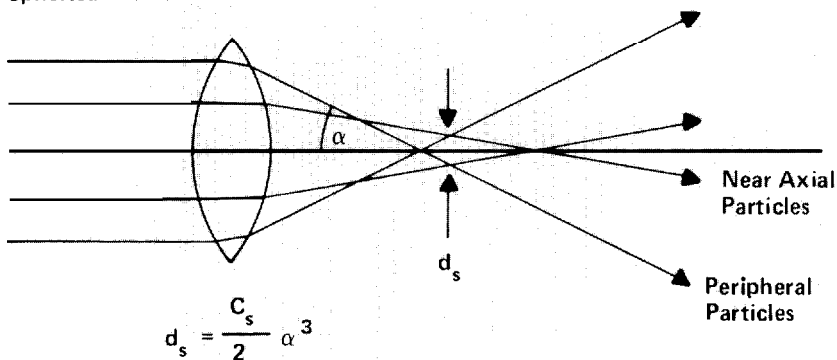


**Fig. 7. Spherical aberration.** The lens focuses ions far from the optical axis more strongly than those near the optical axis. Because of these spherical aberrations, the area of the focused spot can be no smaller than the “disk of least confusion” of diameter  $d_s$ . The angle  $\alpha$  is the divergence half-angle of the focused spot. The calculated value of the spherical aberration coefficient  $C_s$  for the superconducting solenoid lens is 14 centimeters.

### Chromatic Aberration

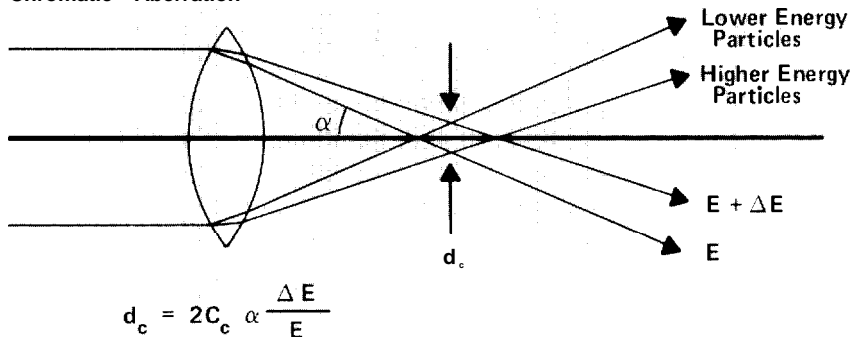


**Fig. 8. Chromatic aberration.** The lens focuses ions with higher energy less strongly than those with lower energy. These chromatic aberrations produce a focused spot with a diameter  $d_c$ . The calculated value of the chromatic aberration coefficient  $C_c$  for the superconducting solenoid lens is 9.3 centimeters.

affect the measurements if the beam remains in focus on the specimen suggests another solution. By changing the focal length of the final lens when the beam energy changes, the spot could be kept in focus and chromatic effects eliminated.

Because of its large inductance, the superconducting solenoid lens cannot be modulated rapidly enough to compensate for the changing incident energy. However, a small electrostatic-quadrupole triplet between the object slit and the solenoid lens could be. We hope to add such a small dynamic focusing element to the Los Alamos microprobe to compensate for the short-term beam-energy fluctuations of the accelerator. The signal to modulate the triplet would be derived from

the energy-regulating slits of the accelerator.

The Los Alamos nuclear microprobe is currently being used with currents of 1 to 20 nanoamperes, spot diameters of 3 to 10  $\mu\text{m}$ , and energy regulation of 5 parts in  $10^4$ . Its design has increased the attainable current densities and data-acquisition rates of such instruments. Table II compares the characteristics of the Los Alamos probe and those of similar instruments around the world.

### Data-Acquisition System

The data-acquisition system is outlined in Fig. 10. The beam spot has a fixed position, and piezoelectric drivers move the sample

TABLE II

## COMPARISON OF NUCLEAR MICROPROBES

System	Magnification		Maximum Acceptance of Final Lens				Phase Space ( $\mu\text{m}^2 \text{ mrad}^2$ )	Drift Space (m)	Focused spot Dimensions	Current Density in Focused Spot ( $\text{pA}/\mu\text{m}^2$ )
	$M_x$	$M_y$	x ( $\pm\mu\text{m}$ )	y ( $\pm\mu\text{m}$ )	$\Delta\theta_x$ ( $\pm\text{mrad}$ )	$\Delta\theta_y$ ( $\pm\text{mrad}$ )				
Harwell "Russian Quad" <sup>a</sup>	0.18	0.18	8.5	8.5	0.62	0.4	18	3.9	---	---
Heidelberg Doublet	0.21	0.038	7	40	0.7	0.39	76	1.9	1.5- $\mu\text{m}$ diam	30
Karlsruhe Doublet	0.43	0.034	3.5	44	1.17	0.47	83	2.7	2.5- $\mu\text{m}$ diam	60
Harwell Triplet	0.114	0.053	13.2	28.4	0.26	0.64	52	3.9	2 by 3 $\mu\text{m}^2$	150
Los Alamos Superconducting Solenoid	0.1	0.1	15	15	2	2	900	1.1	2.5- $\mu\text{m}$ diam	500

<sup>a</sup>This system produced the first focused probe.

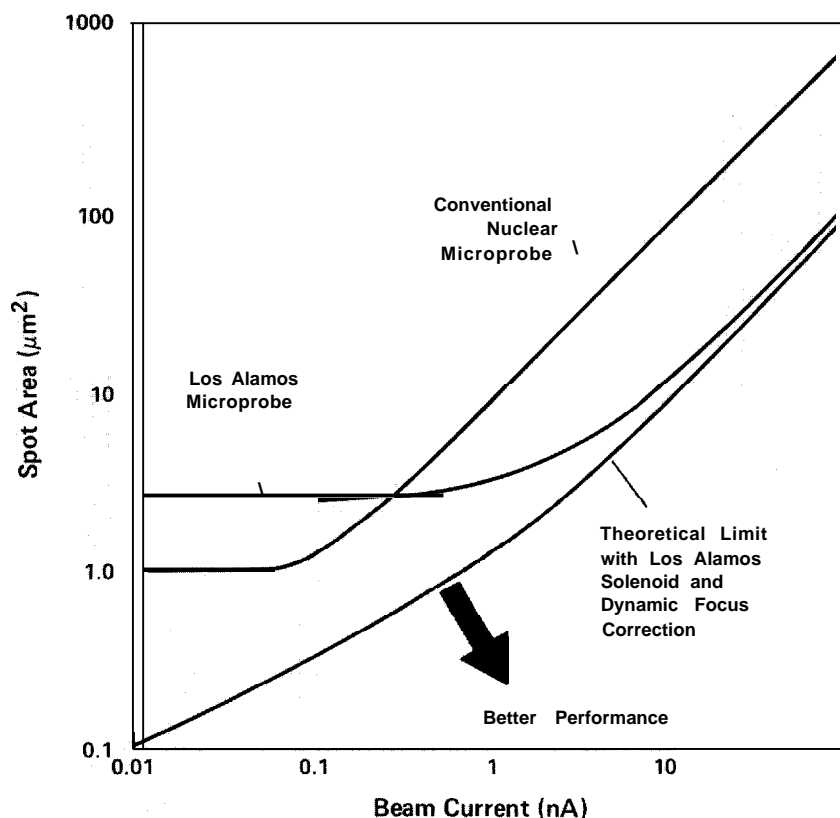


Fig. 9. Demonstrated performance of the Los Alamos superconducting solenoid lens compared with that of conventional nuclear microprobe. The curves for the superconducting solenoid lens include the effects of both chromatic and spherical aberrations. These were calculated analytically by approximating the solenoid's magnetic field with that of a Glaser field. Chromatic aberrations dominate the increase in spot diameter. Improved energy regulation would decrease this effect but is very difficult to accomplish. Dynamic focusing could compensate for chromatic aberrations by altering the focal length of the final lens as the beam energy changes. With dynamic focusing currents of a few hundred picoamperes could be focused into a spot less than a micrometer in diameter.

wheel in a computer-generated raster pattern. The sample wheel is visible in the photograph of the irradiation chamber (Fig. 11). Data at each sampling area are acquired for a preset integrated charge of incident ions. Spectral information from the detectors is recorded on magnetic tape for permanent storage and later analysis. Analysis of the data can provide background subtraction, position averaging, one-dimensional line scans, two-dimensional elemental maps, and elemental depth profiles. The software needs are more than enough to test one's imagination and stamina as a programmer.

The fixed-beam design was intended for semiconductor and metallurgical applications where localized heating was not expected to be a problem. However, fast deflection of the beam would be desirable for specimen positioning and beam focusing to minimize localized heating in specimens of low thermal conductivity. Addition of this capability to the beam line is under study. The instrument is acquiring the features of a scanning electron microscope, but the particles with which it probes give it different analytical capabilities.

### Nuclear Microprobe Applications

To biologists, ion-induced x-ray emission is of interest not only because of its sensitivity of 1 to 10 parts per million but also because of its 1- $\mu\text{m}$  resolution. The higher sensitivity of the nuclear microprobe compared with that of the electron microprobe provides more information about the composition of single cells. At a resolution of 1  $\mu\text{m}$ , elements in the nucleus of a cell can be resolved from those in the cytoplasm. The ultimate usefulness of the nuclear microprobe in biology will be determined by the

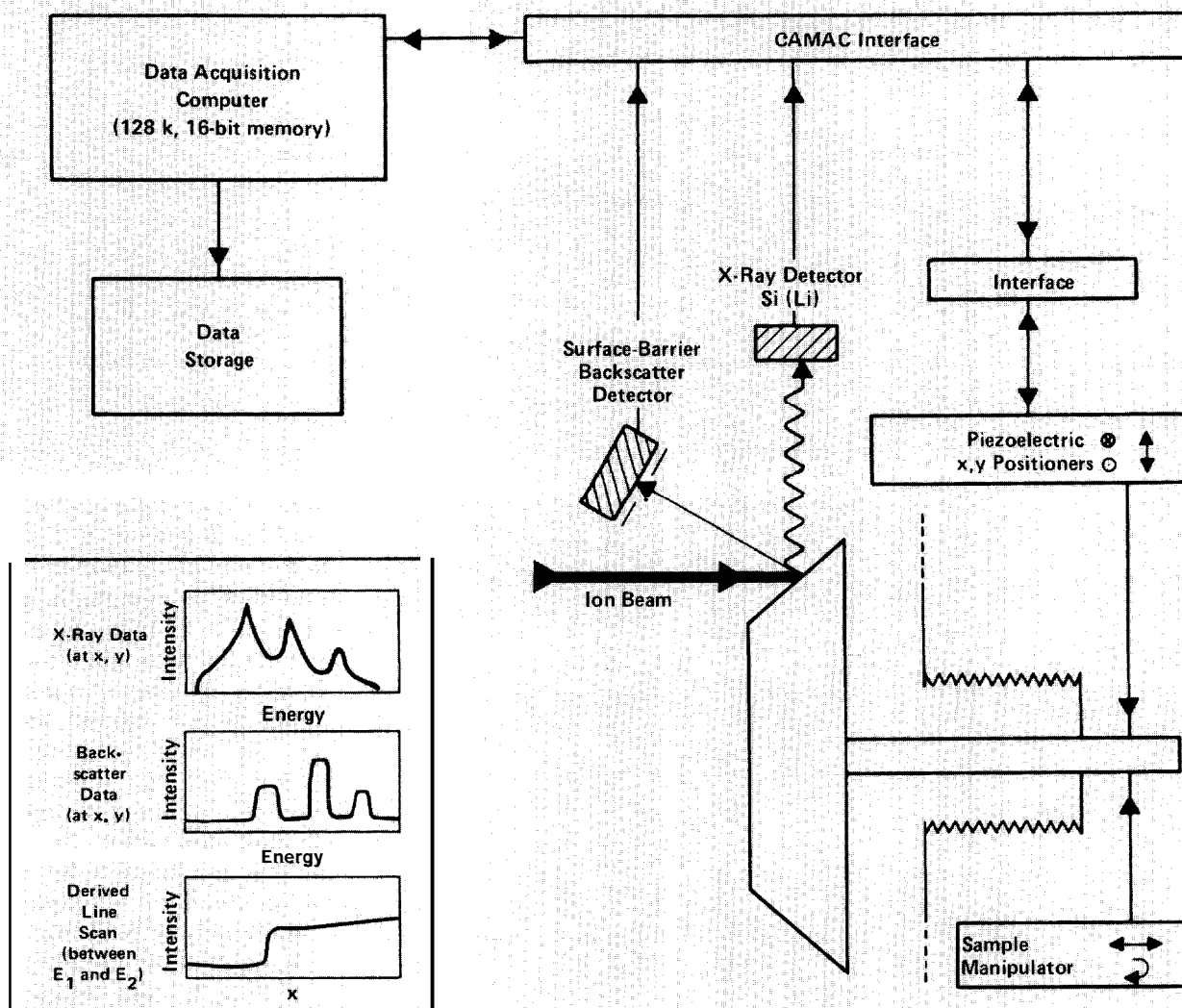


Fig. 10. Data-acquisition system of the Los Alamos nuclear microprobe. Computer-controlled piezoelectric drivers move the sample in a raster pattern relative to the fixed ion beam. At each point x-ray and/or backscattering signals from the detectors are recorded by the computer for a preset integrated

charge of incident ions. During data acquisition the computer operates as a multichannel analyzer with up to 72 gates (energy windows) on the two incoming signals. The figure also shows various ways in which the data can be displayed.

susceptibility of biological samples to radiation damage. So far, no special efforts have been made to minimize specimen damage. A systematic look at the problems of specimen contamination during sample preparation and elemental migration during analysis is needed to push the biological applications beyond the studies already performed. Measuring and limiting the movement of ions at a concentration of 10 parts per million over distances on the order of 1  $\mu\text{m}$  will not be simple.

To geologists or geochemists, the utility of the nuclear microprobe arises from its sensitivity to trace elements and its ability to

analyze individual inclusions in a complex mineral. When sensitivities greater than 1000 parts per million are needed, the usual procedure has been to use a bulk technique, such as neutron activation or x-ray fluorescence. These techniques are not well suited to study of individual grains or small inclusions in the host mineral. But with the spatial resolution and sensitivity of the nuclear microprobe, we can determine the partitioning of trace elements among coexisting minerals. This information contains important clues about the rock's formation.

For example, by studying the minor amounts of zirconium oxide ( $\text{ZrO}_2$ ) in il-

menite and ulvospinel in lunar basalts, the equilibrium temperatures and cooling rates of the host rocks can be determined. The Heidelberg proton microprobe has been used to study ilmenite grains from the Apollo 17 mission. These rather special samples provided a test for the sensitivity of the nuclear microprobe. Zirconium was not detected by an electron beam but was readily apparent with the 2-MeV protons of the Heidelberg probe. Similarly, the use of zircons in geochronology studies requires a knowledge of thorium, lead, and uranium distributions in zircon grains. The proton microprobe has the sensitivity and spatial

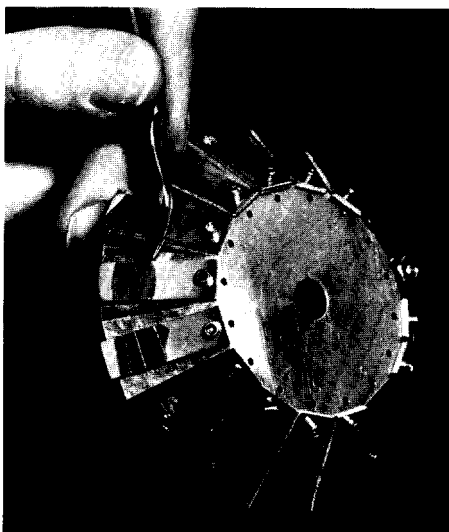
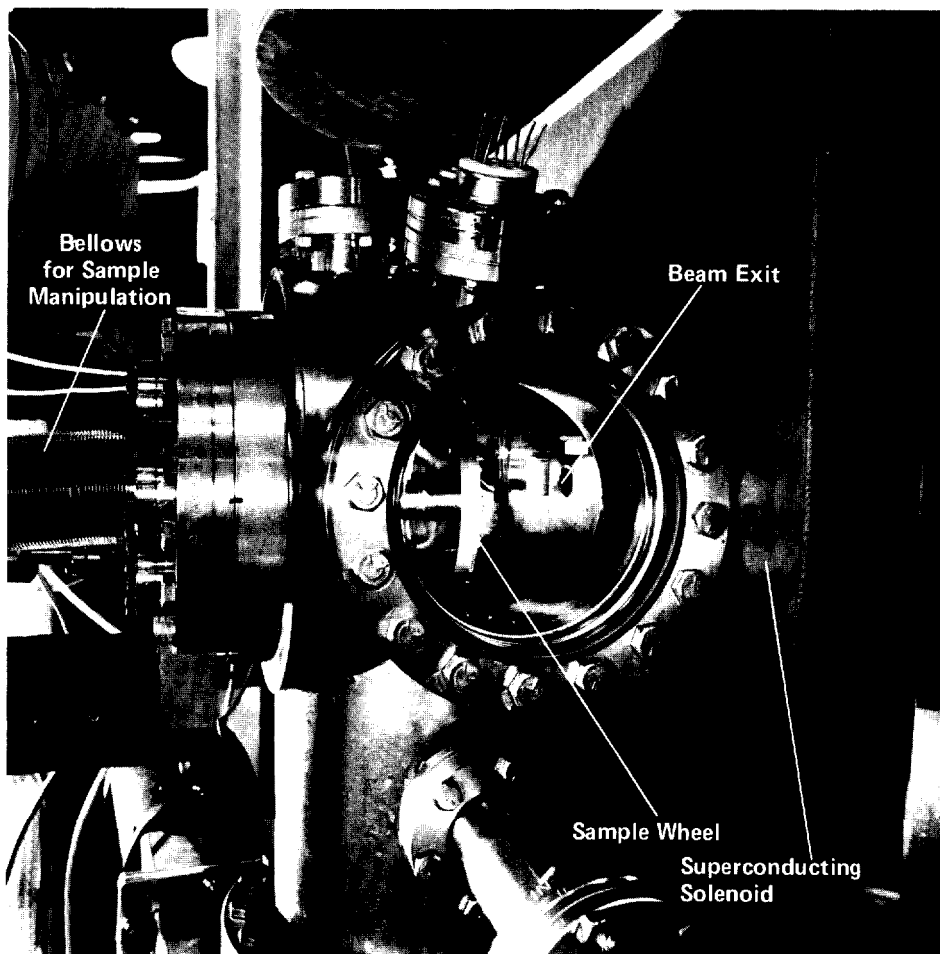


*Fig. 11. Top. The microprobe sample wheel with mounts for sixteen samples. Bottom. Target chamber of the nuclear microprobe. The sample wheel and the beam-line exit are visible through the chamber window. The housing of the solenoid lens and the bellows for the piezoelectric drivers and sample manipulator are also visible.*



resolution required to follow the 100-parts-per-million lead concentrations in individual zircons.

The most well-developed applications of the nuclear microprobe are metallurgical. This is understandable since the first nuclear microprobe was developed at Harwell, where metallurgical problems associated with nuclear reactors are a primary concern. Hydrogen embrittlement of metals is one such problem, and its understanding requires information about the distributions of hydrogen and deuterium. This information was obtained by detecting nuclear reaction products from the nuclear microprobe. Other problems studied at Harwell include carbon distributions in welds before and after heat treatment, the role of nitrogen in brittle cracking of zirconium alloys, the influence of boron on the ductility of irradiated steels, and beryllium diffusion in metals corroded by copper oxidation.

At Los Alamos the nuclear microprobe has opened up new possibilities in the analysis of thin films, electrochemical systems, and geologic materials. These analyses are discussed in the applications that follow.

Even though the first nuclear microprobe has been in existence for almost ten years, the instrument is still "new." Applications are in their infancy, and many possible uses remain to be explored. An air of excitement and discovery attends the first look at a new specimen. Surprises are frequent in the world below 10  $\mu\text{m}$ , where preconceived ideas are often found to be incorrect. Fortunately, the relative ease and certainty of the data analysis leave little chance for misconceptions to survive. The ease and certainty rest on the great body of experimental and theoretical knowledge about interactions of few-MeV light ions with matter. Nuclear microprobe experiments can apply this knowledge to the study of "real world" problems and fundamental problems in geochemistry, biology, and materials science. The mature science of nuclear physics is being used in ways unimagined by its pioneers. ■

# *Trace-Element Analysis of Geologic Materials*

Geologic materials are complex, heterogeneous mixtures of minerals, often small grained and each with a different composition. Study of these materials demands an instrument capable of providing spatially resolved, *in situ* elemental analyses. The electron microprobe is adequate to the task if a sensitivity of 1000 parts per million is sufficient. The nuclear microprobe, which is capable of analysis at the level of 10 parts per million, can measure trace-element distributions in individual mineral grains in addition to major and minor elements. Experiments of this type were not before possible.

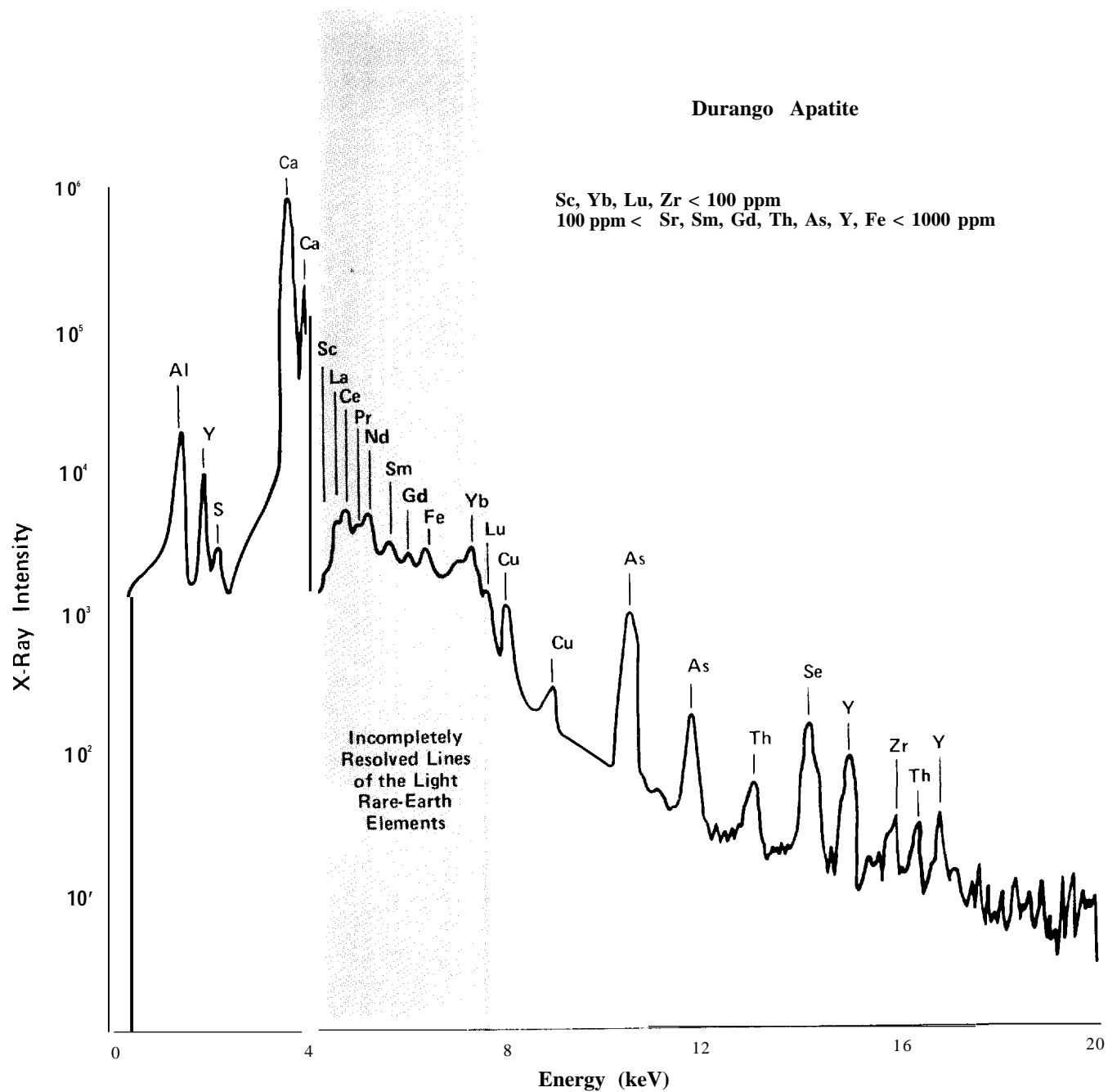
For example, consider the problem of determining the relative ages of meteorites, information important to theories of the origin and evolution of the solar system. Relative ages of meteorites can be deduced from the inferred abundances of the isotope plutonium-244. (Plutonium-244 is now extinct; its former abundance in a meteorite can be inferred, for example, from the abundance of its xenon decay product.) Since plutonium has no stable or very long-lived isotopes, this dating technique requires normalizing the plutonium abundance to that of another element in the meteorite. There is evidence suggesting that the geochemical behavior of plutonium is similar to that of uranium and the light rare earths, and therefore one of these elements is usually chosen for the normalization. But the validity of the normalization hinges on whether plutonium and the normalized element undergo similar fractionation during mineral formation. Experiments on synthetic geologic samples have shown that the magnitude of plutonium fractionation is between those of uranium and of the light rare earths. This fact allows application of a proposed "bracketing theorem" leading to the conclusion that if uranium and the light rare earths, when normalized to cosmic abundances, are not fractionated relative to each other in a particular meteoritic mineral, then the plutonium also was not fractionated relative to uranium and the light rare earths. The nuclear microprobe can select those meteorites suitable for plutonium-244 dating by determining that

their contents of uranium and light rare earths are unfractionated.

The nuclear microprobe can also be used to study partitioning of trace elements in metal-sulfide-silicate systems. By comparing trace-element concentrations in the rocks of planetary objects with the results of synthetic partitioning experiments, we can obtain information about the differentiation of the planets into metallic cores and silicate mantles. Previously, such studies were hampered by the low concentrations of siderophile (metal-loving) and chalcophile (sulfide-loving) elements in silicate phases, lithophile (silicate-loving) and chalcophile elements in metal phases, and siderophile and lithophile elements in sulfide phases and by the necessity of physically separating the various phases before measuring the trace-element concentrations.

We have undertaken a series of experiments to test the limits of the nuclear microprobe for measuring trace-element concentrations in minerals. The accompanying figure shows the x-ray spectrum from Durango apatite, a calcium fluorophosphate that contains a large number of rare earths and typifies the complexity of geologic materials. Although the nuclear microprobe is able to detect the rare earths at a concentration of 10 parts per million, the solid-state x-ray detector cannot resolve the peaks that overlap. A focusing crystal spectrometer has the necessary energy resolution to resolve these peaks but only about one-thousandth the efficiency of the Si(Li) detector. To overcome this difficulty, the microprobe current could be increased by making use of the high phase-space acceptance of the solenoid. A crystal x-ray spectrometer is being added to the Los Alamos nuclear microprobe to combine high-resolution x-ray spectroscopy with spatially resolved trace-element sensitivity.

*This work was performed in conduction with Timothy M. Benjamin and Pamela Z. Rogers of Los Alamos and Dorothy Woolum of the California Institute of Technology.*



*Results of a nuclear microprobe analysis of Durango apatite, a mineral containing a large number of rare earths. X-ray*

*emission was induced by a beam of 3-MeV protons.*

# Catalyst Stability in Fuel-Cell Electrodes

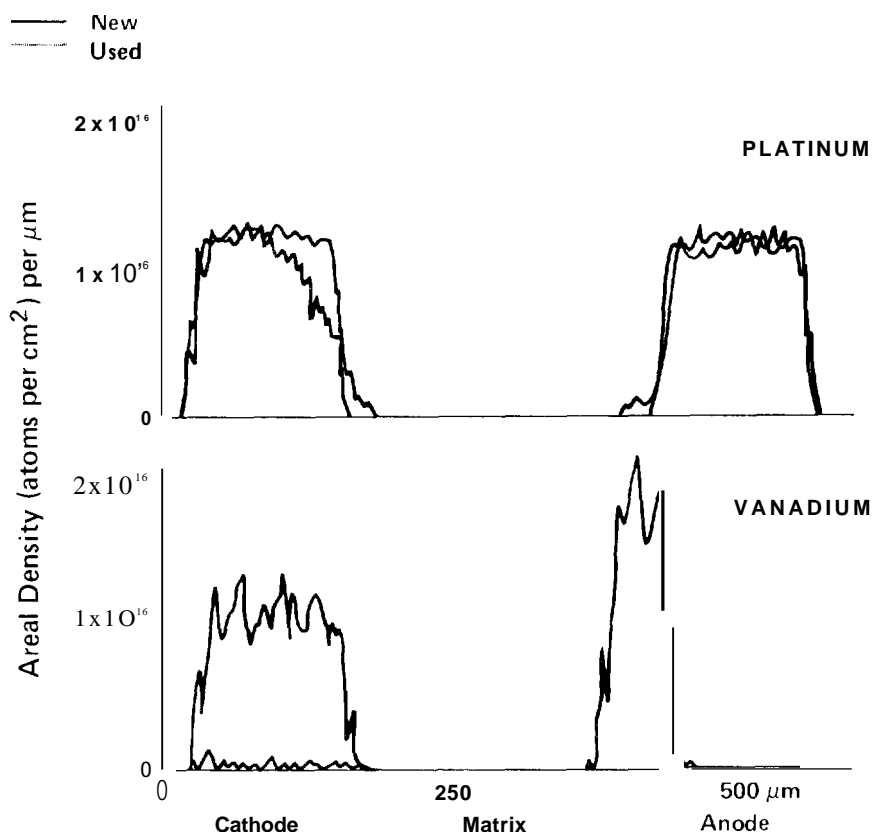
## Applications

A fuel cell is a device that converts chemical energy directly to electrical energy, thus bypassing the usual intermediate and energy-wasting conversions to thermal and mechanical energy. A fuel cell based on the reaction of hydrogen and oxygen was conceived and constructed as early as 1839, but the idea was not pursued with much enthusiasm until more than a hundred years later. In recent times the development of fuel cells has been spurred by the search for more efficient and nonpolluting sources of electricity.

Basically, the hydrogen-oxygen fuel cell consists of porous electrodes separated by an electrolyte. Hydrogen and oxygen diffuse through the anode and the cathode, respectively, and undergo reactions that create a potential difference across the cell. At the anode hydrogen molecules dissociate into atoms and then release electrons. The hydrogen ions flow to the cathode through the electrolyte, and the electrons flow through the external circuit. At the cathode oxygen molecules dissociate and accept electrons from the external circuit. The hydrogen and oxygen ions then combine to form water.

To achieve high rates of dissociation and oxidation or reduction of the gases, a platinum catalyst is embedded in the electrodes. Platinum is costly, and, further, its activity for oxygen reduction at the cathode is less than ideal. An attempt has been made to reduce the amount of platinum required and increase the cathode activity by using an intermetallic platinum-vanadium compound as the cathode catalyst. The intermetallic compound shows an initial activity for oxygen reduction greater than that of platinum, but during operation its activity decreases to that of the pure metal.

The performance of a fuel cell may degrade during use, possibly because of loss of the catalyst from the electrodes. In fact, such losses are to be expected since the cathode operates at a potential close to the oxidation potential of the catalyst. We studied the migration process with the microprobe by



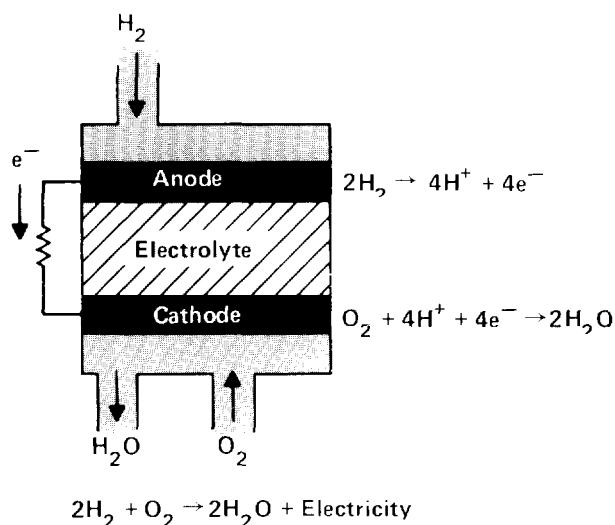
*Distribution of catalyst in the electrodes of a fuel cell before use and after about 3000 hours of operation. Initially, the cathode and anode contained catalysts of platinum-vanadium and pure platinum, respectively. Note the loss of vanadium from the cathode and its buildup in the matrix near the anode of the used fuel cell.*

measuring the catalyst depth distributions in new and used electrodes. The signals detected were backscattered protons from an incident beam of 3-MeV protons. To obtain the depth distribution throughout the regions where the chemical reactions take place, we made a small-angle cut through the electrode and performed a line scan across the bevel.

For electrodes containing a catalyst of

pure platinum, the catalyst was found to be fairly stable, although there was some loss of catalyst from the cathode after several thousand hours of operation.

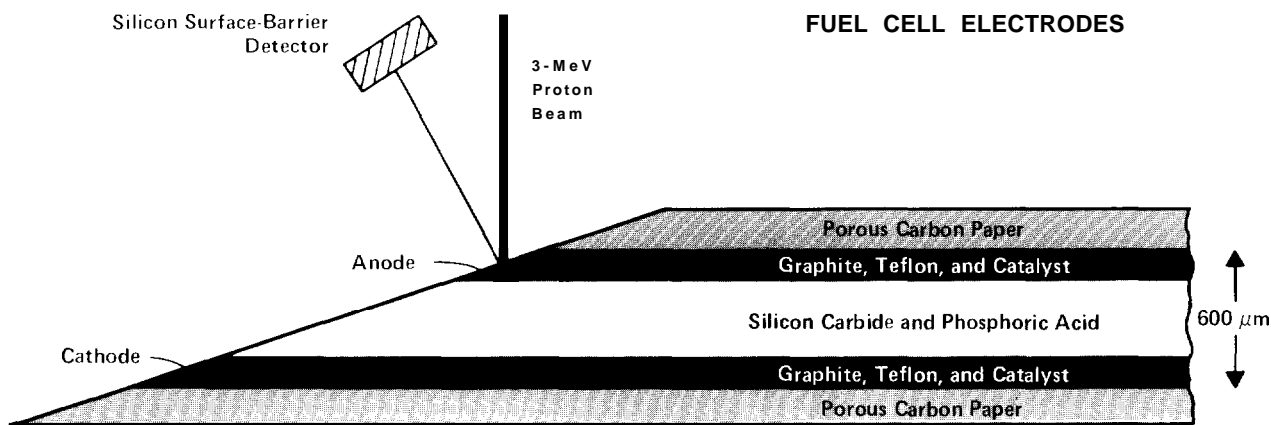
More interesting results were obtained for electrodes with platinum-vanadium as the cathode catalyst and platinum as the anode catalyst. In this case we determined simultaneously the depth distributions of



*Schematic diagram of a hydrogen-oxygen fuel cell.*

platinum, vanadium, silicon, phosphorus, oxygen, fluorine, and carbon in the cathode, anode, and matrix. (The accompanying figure gives the depth distributions of platinum and vanadium.) Our results showed that the vanadium component of the platinum-vanadium catalyst is not stable. The vanadium dissolves in the phosphoric acid, migrates through the silicon carbide matrix, and accumulates near the anode. We are now studying several other intermetallic catalysts with a view to improved and more stable fuel-cell performance.

*This work was performed in conjunction with Philippe J. Hyde and S. Srinivasan of Los Alamos.*



*Experimental setup for using the nuclear microprobe to determine the distribution of catalyst in a fuel-cell electrode of current design. The concentration of catalyst in the electrodes is about 1 part in 2000. The Teflon particles prevent flooding of the electrodes by the phosphoric acid electrolyte. The*

*chemical reactions take place close to the three-phase regions where the gases react on the solid graphite-catalyst surface and the liquid electrolyte provides mobility for the hydrogen ions. The conducting carbon paper and graphite provide a path for the electrons.*

# Densities of Thin-Film Targets

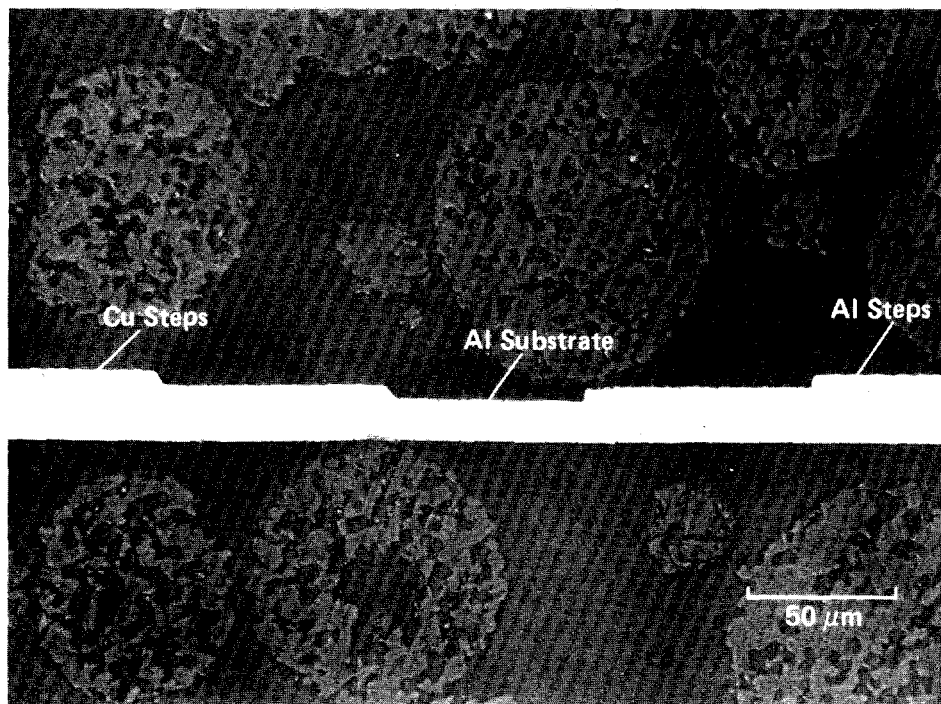
## Applications

For several years Los Alamos and Livermore scientists have been using sharply focused high-power, pulsed lasers to produce high-velocity shock waves in thin-film targets. The shock waves create the intense pressures and high temperatures characteristic of the detonation of weapons and other explosives. The purpose of the experiments is to determine equations of state (the relationship among pressure, temperature, and density) for the target materials under these extreme conditions.

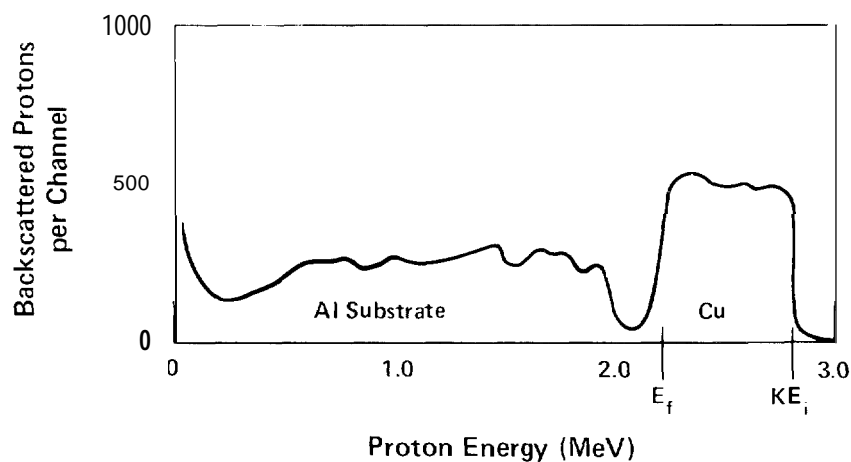
The experiments pose many difficulties, and among them is the need for an accurate measurement of the initial density and uniformity of the targets, which are fabricated by evaporating thin films onto an aluminum substrate. The nuclear microprobe provides a way to measure areal density (mass per unit area) *in situ* and nondestructively. The areal density, which is related to the width of the film's backscattering peak, is then combined with an independent thickness measurement to yield the density with an accuracy of 1 per cent.

Using a few-nanoamperes current of 3-MeV protons focused to a spot 10 micrometers in diameter, we measured the areal density and uniformity of gold, silver, copper, and aluminum targets. [A thin (0.025 micrometer) marker layer of gold between the substrate and the aluminum film permitted a measurement of the aluminum target on the aluminum substrate. The areal density of the aluminum film is then deduced from the observed energy shift of the gold backscattering peak.] In all cases, the areal densities varied from one 10-micrometer-diameter spot to another by less than 1 per cent. The nuclear microprobe is perhaps the only way to obtain such localized information about the areal density. And the superconducting solenoid of the microprobe easily produces the currents and focused beam sizes required to obtain the data in a reasonable time.

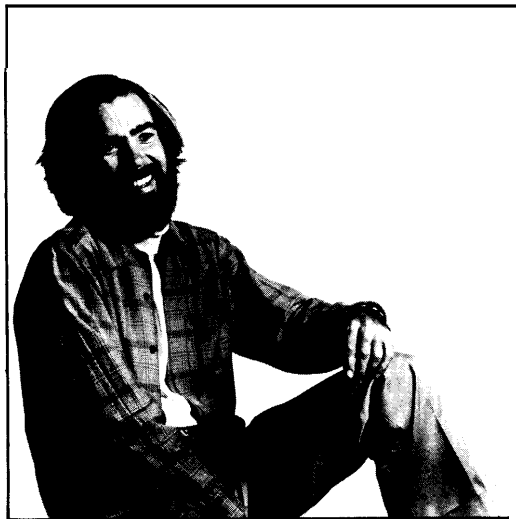
*This work was performed in conjunction with Lynn R. Veaser of Los Alamos.*



*Optical micrograph of the cross section of a thin-film target for equation-of-state studies with lasers.*



*Spectrum of protons backscattered from a target region containing a 5-micrometer-thick copper film on the aluminum substrate. This spectrum is typical of all those from films heavier than the aluminum substrate. The areal density of the copper film is related to  $KE_1 - E_f$ .*



**Carl J. Maggiore** earned his Bachelor of Science from Creighton University in 1965 and his Ph.D. in nuclear physics from Michigan State University in 1972. While working at Mt. Sinai Medical School in their Environmental Science Laboratory, he developed instrumentation for microanalysis of small (less than 0.1- $\mu\text{m}$ -diameter) particles and studied transmission and scanning microscopy of particulate in environmental samples and in human organs to determine the health effects of asbestos. Before coming to Los Alamos, he was manager of the X-Ray Analytical Division at Princeton Gamma-Tech, Inc. Currently he is a staff member in the Electronics Division's Research and Development Group. His work there includes developing near-surface analytical techniques involving ion beams for applications in solid-state devices, in electrochemistry, and in catalysis. He is particularly interested in combining channeling/blocking of ion beams with ultra-high-vacuum surface techniques to determine the effects of geometry on the chemical reactivity of surfaces.

## ACKNOWLEDGMENTS

The author acknowledges the help and support of the Laboratory's Van de Graaff Group and extends special thanks to Mark G. Hollander, Joseph R. Tesmer, Ray V. Poore, and David R. Schmitt.

## Further Reading

O. Meyer, G. Linker, and F. Kappeler, Eds., *Ion Beam Surface Layer Analysis* (Plenum Press, New York, 1976), 2 vols.

Wei Kan Chu, James W. Mayer, and Marc-A. Nicolet, *Backscattering Spectroscopy* (Academic Press, New York, 1978).

J. A. Cookson, "The Production and Use of a Nuclear Microprobe of Ions at MeV Energies," *Nuclear Instruments and Methods* 165,477-508 (1979).

C. J. Maggiore, "Materials Analysis with a Nuclear Microprobe," in *Scanning Electron Microscopy/1980/1* (Scanning Electron Microscopy, Inc., P. O. Box 66507, AMF O'Hare, Illinois 60666) pp. 439-454.

C. J. Maggiore, "The Los Alamos Nuclear Microprobe with a Superconducting Solenoid Final Lens," *Nuclear Instruments and Methods in Physics Research* 191, 199-203 (1981). This volume of *Nuclear Instruments and Methods in Physics Research* is titled "Ion Beam Analysis" and is devoted entirely to that topic.

